

# UC Berkeley

## UC Berkeley Previously Published Works

### Title

Hydrophobic solvation of Gay-Berne particles in modified water models

### Permalink

<https://escholarship.org/uc/item/4j33v2x3>

### Journal

The Journal of Chemical Physics, 128(10)

### ISSN

0021-9606

### Authors

Head-Gordon, Teresa  
Lynden-Bell, Ruth M

### Publication Date

2008-03-14

### DOI

10.1063/1.2837289

Peer reviewed

# **HYDROPHOBIC SOLVATION OF GAY-BERNE PARTICLES IN MODIFIED WATER MODELS**

**Teresa Head-Gordon<sup>1\*</sup> and Ruth M. Lynden-Bell<sup>2,3</sup>**

<sup>1</sup> Department of Bioengineering, University of California, Berkeley, CA 94720

<sup>2</sup>Atomistic Simulation Centre, School of Mathematics and Physics, Queen's University,  
Belfast BT7 1NN, UK.

<sup>3</sup>University Chemical Laboratory, Cambridge University, Cambridge CB2 1EW, UK

## **ABSTRACT**

The solvation of large hydrophobic solutes, modeled as repulsive and attractive Gay-Berne oblate ellipsoids, is characterized in several modified water liquids using the SPC/E model as the reference water fluid. We find that small amounts of attraction between the Gay-Berne particle and any model fluid results in wetting of the hydrophobic surface. However significant differences are found among the modified and SPC/E water models and the critical distances in which they dewet the hydrophobic surfaces of pairs of repulsive Gay-Berne particles. We find that the dewetting trends for repulsive Gay-Berne particles in the various model liquids correlate directly with their surface tensions, the widths of the interfaces they form, and the openness of their network structure. The largest critical separations are found in liquids with the smallest surface tensions and the broadest interfaces as measured by the Egelstaff-Widom length.

**\*Corresponding author**

## 1. INTRODUCTION

It is well appreciated that hydrophobic interaction is an important thermodynamic driver for protein self-assembly into functional native states. At the same time, hydrophobic interactions are also partly responsible for proteins sacrificing stabilizing intra-chain contacts in favor of inter-molecular interactions that can possibly stabilize aggregates or protein complexes in some special cases. One possible molecular reason for this difference is the role of aqueous environment on different spatial lengthscales with respect to a water molecule diameter. The hydrophobic interaction relevant for protein folding is usually within the “wetting regime” dominated by entropic effects, and in which hydrophobic solvation free energy scales with volume<sup>1-4</sup>. It pertains to small hydrophobic groups of size similar to a water molecule. However, the hydrophobic interaction relevant for protein complexation may be within the “dewetting regime” dominated by enthalpic effects of forming a vapor-liquid interface near more extended hydrophobic surfaces so that solvation free energies scale with surface area and not volume<sup>1,2,5</sup>. Such an example was recently reported for protein complexation of the melittin tetramer<sup>6</sup>, although hydrophobic induced dewetting was found not to be the mechanism for collapse of a multi-domain protein<sup>7</sup>.

The theoretical framework for quantitatively describing the thermodynamics of solvation for small hydrophobic solutes, starting with the seminal work of Pratt Chandler theory<sup>3</sup> and its generalization to Information theory<sup>4</sup>, have shown that the inherent structural correlations of bulk water result in tighter voids relative to other organic liquids<sup>8,9</sup>, well-described by solvent density fluctuations which are Gaussian<sup>1,2,4</sup>. This tighter network structure in turn exerts a larger squeezing force that explain water’s solvophobicity<sup>8,9</sup>, although the water network can also reorganize with some entropic penalty to stabilize small hydrophobic species in configurations that don’t show demixing<sup>3,4</sup>.

By contrast the water network can not reorganize so readily in the presence of a macroscopically large hydrophobic interface, and therefore must break hydrogen-bonds to accommodate its presence<sup>1,2</sup>. An “unbalancing” force<sup>10,11</sup> develops near extended surfaces in which the solvent molecule pulls away from the interface with which it cannot gain favorable interactions, creating a thin vapor layer at the surface to maximize interactions with the higher density phase. When there are a pair of such hydrophobic plates, two liquid-gas interfaces are formed, and the liquid will remain in the gap between the surfaces until a critical separation is reached, at which point the unfavorable interfacial energy is no longer compensated by the binding energy of the bulk liquid, and the liquid phase becomes metastable<sup>11-13</sup>.

At this critical separation or smaller, the unstable confined liquid can be expelled from between the plates following fluctuations that nucleate the complete drying event. Mechanistic molecular dynamics studies for various model liquids suggest that the transition state for this rare event is the appearance of a vapor tube that connects the two extended vapor layers<sup>13</sup>. Recent studies indicate the resulting free energy barrier is kinetically manageable so that the induced attraction between plates is observed to occur on laboratory-accessible time scales for purely solvophobic surfaces, although small amounts of surface attraction can make it kinetically impossible for drying to occur<sup>14,15</sup>.

In this work we use SPC/E and several modified water liquids that have different network organizations to evaluate the liquid density profiles between two large hydrophobic solutes, modeled as repulsive and attractive Gay-Berne (GB) oblate spheroids<sup>12,16</sup> (see schematic in Figure 1). The water-like liquids were constructed by making various modifications to the intermolecular forces of the SPC/E model by either reducing the hydrogen bond strength so that the liquid becomes more like a simple Lennard-Jones liquid (the H15 and H30 models)<sup>17</sup>, or altering the network

structure by changing the bond angle (the B90 and B60 models)<sup>18</sup>, or constructing an isotropic model with the same two-body structural correlations, but quite different three body correlations (the ISO model)<sup>19-21</sup>. We find that small amounts of attraction between the GB particle and any liquid model examined here results in wetting of the two hydrophobic surfaces. More interestingly we find that the critical separation for dewetting between pairs of repulsive Gay-Berne particles varies with the model liquid. This variation correlates directly with surface tension, interface width, and openness of the network structure. The largest critical separations are found in liquids with the smallest surface tensions and the largest Egelstaff-Widom length.

## 2. MODELS AND METHODS

### 2.1. Models

The reference intermolecular potential is the SPC/E model<sup>22</sup>, whose energy  $\Phi$  is written as a sum of pairwise intermolecular interactions and can be expressed as

$$\Phi = \sum_{pairs} V^{LJ}(r_{ij}) + V^{ES}(r_{ij}, \Omega_{ij}) \quad (1)$$

where  $r_{ij}$  is the separation between oxygen atoms on molecules  $i$  and  $j$ , and  $\Omega_{ij}$  describes the relative orientation of the molecules. The Lennard Jones interaction  $V^{LJ}(r)$  is

$$V^{LJ}(r) = 4\epsilon_{LJ} \left[ \left( \frac{\sigma}{r} \right)^{12} - \left( \frac{\sigma}{r} \right)^6 \right] \quad (2)$$

where  $\sigma$  is the value of  $r$  where the potential is zero, and  $\epsilon_{LJ}$  determines the energetic scale of the pair interaction. The electrostatic interaction acts between all pairs of charges,  $z_m$  and  $z_n$ , on oxygen and hydrogen atoms belonging to different molecules

$$V^{ES}(r) = \frac{\zeta_\mu \zeta_\nu}{4\pi\epsilon_0 r} \quad (3)$$

where  $\epsilon_0$  is the vacuum permittivity. In this model of “real water”, the hydrogen bonds are described by the electrostatic terms which favour local tetrahedral structure as the bond angle is equal to the tetrahedral angle.

In the hybrid family of models, the relative weights of the Lennard-Jones and electrostatic components are changed by scaling the Lennard-Jones term by a factor  $\lambda$ , so that the potential energy  $\Phi$  becomes

$$\Phi = \sum_{pairs} \lambda V^{LJ}(r_{ij}) + V^{ES}(r_{ij}, \Omega_{ij}) \quad (4)$$

The two hybrid liquids considered in this paper are H15 with  $\lambda=1.5$  and H30 with  $\lambda=3.0$ . While this family of potentials have very similar well depths for pairs of molecules<sup>17</sup>, the values of  $\lambda$  were chosen to span the dramatic changes in local structure that were found previously<sup>17</sup>. Given the shift in relative weights of the LJ and electrostatic terms, the hydrogen bond strengths (as measured by the electrostatic component of the dimer energy) are reduced to 87% and 69% for H15 and H30, respectively, relative to SPC/E water. Table 1 summarizes the values of the parameters for the hybrid family.

In the bent family of models the bond angle is reduced while keeping the same SPC/E charges. The two liquids considered in this family are a model with a bond angle of  $90^\circ$  (B90) and a model with a bond angle of  $60^\circ$  (B60), and the dipole moment of SPC/E is retained by reducing the bond lengths.

The values of the Lennard-Jones  $\sigma$  parameters of the two models are changed to obtain the same number densities at 298K and 1 atmosphere pressure, while the  $\epsilon_{LJ}$  parameters are unchanged. Table 1 summarizes the values of the parameters for the bent family. The result of the change in bond angle is to destroy the tetrahedral network, even though there are still hydrogen bonds to produce a network of chains of water molecules<sup>18,23</sup>.

The interaction potential of the isotropic model differs significantly in functional form from all of the model liquids described thus far. It is constructed to have the same two body radial distribution function as the oxygen-oxygen radial distribution function,  $g_{oo}(r)$ , of SPC/E water at 298K. We solve for the interaction potential using the empirical potential structure refinement (EPSR) procedure<sup>24</sup> in which a chosen reference potential is perturbed by a constraint on the allowed  $g_{oo}(r)$

$$\Phi_i(r) = \Phi_{i-1}(r) + k_B T \ln \left[ \frac{g_{i-1}^{Iso}(r)}{g_{OO}^{TIP4P-Ew}(r)} \right] \quad (5)$$


and then iterated to self-consistency. Unlike the other models, the ISO liquid is not bound and the state point is in the supercritical region. Consequently simulations were carried at the liquid water density corresponding to a very high pressure of  $\sim 9000$  atm.

Large hydrophobic solutes were modeled as two oblate spheroidal Gay-Berne particles (pancake-shaped)<sup>12,16</sup> placed in the cubic box at varying center-to-center distances. The Gay-Berne potential interaction with water comprises

$$V_{GB-w} = 4\epsilon_{HMB} \left[ \left( \frac{\sigma_0}{r - \sigma(\chi; \nu) + \sigma_0} \right)^{12} - \left( \frac{\sigma_0}{r - \sigma(\chi; \nu) + \sigma_0} \right)^6 \right] \quad (6)$$

where  $r$  is the distance between the Gay-Berne particle and the water oxygen,  $\sigma(\chi; \nu)$  is an orientation-dependent Lennard-Jones diameter

$$(7)$$

and  is a function of  $\sigma_{\parallel}$  and  $\sigma_{\perp}$  that define the axial ratio and lengths of the oblate ellipsoid

along the major and minor axes, respectively, and  $\nu$  is the angle between the major axes of the

ellipsoid and the unit vector pointing from the center of the ellipsoid to water's oxygen atom. We used a pair of Gay-Berne particles with  $\sigma_{\parallel} = 1.8343\text{\AA}$ ,  $\sigma_{\perp} = 13\text{\AA}$  (Figure 1) and for each size a series of simulations with different separation  $D$  between the two ellipsoids was performed to determine whether the cavity between the plates were either filled with water or were devoid of water. We also performed the simulations with a fully repulsive solute–solvent potential (the first term in Eq. (6)) and with the full potential but varying  $\epsilon_{HMB}$  ranging from the original study value of  $\epsilon_{HMB}=0.5925$  kcal/mol ( $=k_B T$  at 298K) reported by Huang and co-workers<sup>12</sup>, as well as significantly smaller values.

## 2.2. Simulation Protocol

A cubic box with edge length of  $\sim 40.0\text{\AA}$  was filled with 2040 particles or molecules. Molecular dynamics (MD) simulations in either the canonical (NVT) or isothermal-isobaric (NPT) ensembles were performed using both an in-house simulation program and for the hybrid and bent models with a modified version of the DLPOLY code<sup>24</sup>. Constant volume runs used a Nosé Hoover thermostat<sup>26</sup> to control the temperature to 298K with a time constant of 0.5ps, and constant pressure runs used an isotropic Nosé Hoover barostat<sup>26-28</sup> with relaxation times of 0.1ps. The equations of motion were integrated using the velocity Verlet algorithm<sup>29</sup> and with a time step size of 1-3 femtoseconds depending on the model liquid. The intra-molecular geometry ( $r_{OH}$  and  $\theta_{HOH}$ ) was constrained by applying the M\_SHAKE<sup>30,31</sup> and M\_RATTLE<sup>28,32</sup> algorithms using an absolute geometric tolerance of  $10^{-10}\text{\AA}$ . Long range corrections were included for both the Lennard-Jones interactions and virial, and for the electrostatic interactions and virial using the Ewald method<sup>33</sup> with parameters chosen to give a precision of  $10^{-5}$  in the Coulomb energy. The duration of equilibration runs was typically 0.3 nanoseconds, and several production runs between 0.3 and 0.5 nanosecond were completed, with configurations saved every 100fs for further analysis. Surface tensions were calculated as the



difference in the normal and tangential pressures calculated from the kinetic energy and virial equation as outlined in reference [34].

### 3. RESULTS

We find that all modified water models, as well as the SPC/E reference model, fill the gap between the attractive GB particles even at the smallest separation value of  $5.0\text{\AA}$ , which is about as small as will fit a water molecule when the finite thickness of the GB particle is taken into account. For the SPC/E model, this result did not change if the energetic scale of the pair interaction between GB particles and water was changed to  $\varepsilon=0.5\varepsilon_{HMB}$  or  $\varepsilon=0.25\varepsilon_{HMB}$  in Eq. (6). We found no difference in these results if we changed the water model to SPC as per the original study. We have no clear explanation as to why our results do not dewet at the separation values of the Gay-Berne particles to that reported by Huang and co-workers<sup>12</sup>.

However, there is a measurable difference between the separations at which the gap first fills between the purely repulsive Gay-Berne particles in the various modified and reference liquids.. The critical gaps for when the cavities are filled are given in Table 2; below those values the cavities are empty. The trend is that the hybrid model liquids show a decrease in the critical separation for empty cavities while the critical distance increases for the bent model liquids relative to SPC/E, while the isotropic model liquid fills the gap at the smallest of separations. The question is how far one may correlate this dewetting trend among the model liquids with their surface tensions, widths of their liquid-vapor interfaces, and network structures.

Figure 2 shows that there is a strong correlation between the critical separation for dewetting and the surface tension of the liquids, such that liquids with higher surface tensions dewet at closer distances. The variation in the critical separation with liquid is surprisingly large, ranging from 15Å for the B60 model to 10Å for the H30 model while the surface tension changes by a factor of over 4 between these liquids. These results can be discussed in terms of a macroscopic model for a liquid between two flat circular plates developed by Huang et al. using the Grand Potential,  $\Omega^{12}$ . We assume that  $\Delta\Omega=0$  at the critical separation,  $D_c$ , and therefore

$$A_{\text{men}}(D_c) = (\Delta\gamma / \gamma) A_w + (\Delta P / \gamma) V \quad (8)$$

where  $A_{\text{men}}$  is the area of the meniscus between the liquid and the bubble, which depends on the separation between the plates,  $D$ ,  $A_w$  is the total area of wall in contact with the bubble,  $\gamma$  is the gas-liquid surface tension,  $\Delta\gamma$  is the difference of the liquid-solid and gas-solid surface tensions,  $\Delta P$  is the difference in the external pressure and the vapor pressure of the liquid, and  $V$  is the volume of the bubble. Although the shape and hence area of the meniscus can vary with  $\Delta P / \gamma$  for a given separation, for our system the changes in area for this term are of the order of parts per million and can be neglected. Thus the critical separation occurs when the area of the meniscus is equal to  $\Delta\gamma / \gamma$  times the area of the two walls. We conclude from the data in Figure 3 that for these liquids the gas-liquid surface tension changes more rapidly than the solid-liquid surface tension so that the ratio  $\Delta\gamma / \gamma$  changes by a factor of 1.5 when the gas-liquid surface tension changes by a factor of 4.

Figure 3 shows average water densities along the symmetry axis (vertical axis in Figure 1) for three of the solvent models between a pair of Gay-Berne particles separated at different distances. These data are constructed by averaging over a cylinder of radius 6 Å around the symmetry axis. It is seen

that the H30 model sustains a much sharper interface with the Gay-Berne particles (Figure 3a), and even though the binding energy for the H30 model is less favorable than SPC/E (Figure 3b) for the bulk phase, its high surface tension and high critical temperature suggests a molecular reorganization at the interface which does not allow the intrusion of a vapour layer until significantly smaller GB separations. The very low surface tension of the B60 model correlates with the closer proximity of the critical point to the ambient state point studied here and results in a broader interface at the Gay-Berne particle surfaces, with low density reaching out to  $\sim 20\text{\AA}$  before recovery to bulk densities (Figure 3c). This result, combined with its relatively low binding energy that does not favor the bulk phase, the B60 model experiences a dewetting transition at the largest GB separations. The intermediate models in the two families (H15 and B90) show intermediate behavior, while the isotropic model fluid never dewets likely because its liquid is not bound at 1atm pressure.

Egelstaff and Widom made the observation that the product of the gas-liquid surface tension,  $\gamma$ , and the isothermal compressibility,  $\kappa_T$ , a quantity with dimensions of length, was largely invariant over a wide range of metallic and non-metallic liquids in coexistence with their vapor<sup>36</sup>. Possible structural interpretations of the Egelstaff-Widom (EW) lengthscale proposed in [36] and relevant in the context of this study, is that it describes a correlation length at the interface:

$$L = \gamma \kappa_T / 0.07 \quad (9)$$

that measures the decay back to bulk like features in the two phases. Since the variation in the EW lengthscale is so small among many different liquids, between  $0.2\text{\AA}$  and  $0.5\text{\AA}$ , it implies that the liquid-vapor interfaces are sharp since the correlation lengths are only one or two molecular diameters. However, for the mesoscopic systems evaluated here, these molecular differences can be important. Table 2 lists these quantities for the H30, SPC/E, and the B60 models. We find that the

EW length increases from 0.22Å for H30, 0.31Å for SPC/E, and 0.47Å for B60, which correlates with the broadness of the interface widths shown in Figure 3.

Based on the analysis of our artificial liquids in previous work<sup>35</sup>, we determined that the H30 liquid exhibits a sharper distribution of smaller naturally occurring voids in the bulk, while the B60 model (which exhibits a hydrogen-bonded chain network) is biased to larger empty voids in the neat liquid. Furthermore, since the presence of the GB particles drives the formation of the gas-liquid interface when the solvent pulls away from the solid surface, the EW length differences among the liquids suggest that the B60 model will be more strongly perturbed from its bulk-like values in the intervening liquid. Thus it would seem that liquids with more open networks in their equilibrium ensemble and with larger EW lengths would show an increase in the size and or number of voids that could nucleate and network to reach across the intervening bridging liquid with appropriate fluctuations to drive the cavitation event.

This is evident in Figures 4 and 5 that show the probability distributions of cavity occupancy for different sphere sizes, sampled in a volume of  $1.0\text{\AA}^3$  at the midpoint between the Gay Berne particles. We see that near the critical separation distances of the GB particles for the H30 (Figure 4a) and B60 (Figure 5a) solvents that the cavity distributions are bimodal, corresponding to both wetting and dewetting events in the two models. For separations of the Gay Berne particles that are just beyond the dewetting transition, the solvation cavity statistics for the H30 model are Gaussian and look very similar to the bulk fluid (Figure 4b) while the B60 model (Figure 5b) remains non-Gaussian and biased toward low occupancy numbers. The larger EW length of the B60 liquid suggest that these voids are enhanced in the presence of the GB particles, and clearly less so for H30. Empirically we see that for the B60 model that the smaller empty cavity sizes of 3.8Å-4.6Å

exist with some probability, but apparently do not network frequently enough to drive cavitation at these larger separations.

#### 4. DISCUSSION

In recent work we have examined solvophobic behavior of water for small model hydrophobic solutes in three distinct families of modified water models that differ from real water in more subtle ways than when it is contrasted with other normal organic liquids<sup>35</sup>. We found that hard spheres were less soluble for the hybrid and isotropic models when compared to the SPC/E water model due to their tighter network structures, while the bent models showed diminished solvophobic behavior relative to SPC/E due to their looser network structures that favor larger voids. The modified models with tighter network structures showed significant deviations from Gaussian density fluctuations, while the void size distribution of the bent models were better described by Gaussian statistics, similar to SPC/E water.

The dewetting trends correlate well with the trends in small lengthscale hydrophobic character of the model fluids in terms of the value of the contact density maximum,  $G_{max}(r)$ , defined as the hard sphere size at which the ratio of the actual density at the surface of a hard sphere to the average density in the liquid is a maximum (Table 2). The greater is the value of  $G_{max}(r)$ , the larger is the squeezing force to drive the hydrophobic particle into a separate phase. Based on the analysis of our artificial liquids in previous work<sup>35</sup>, larger values of  $G_{max}(r)$  correspond to liquids with smaller naturally occurring voids. Because the H30 model shows the tightest interface, and a network structure with tighter voids and density fluctuations that are more bulk-like, it is the least likely to evaporate at large separations. The B60 model shows the broadest interface, and its non-Gaussian density distributions are biased toward low density regions, consistent with greater ease in

cavitation at larger GB separations. It suggests that liquids with more open networks show an increase in the naturally occurring voids in contact with the hydrophobic surfaces before dewetting occurs.

While the importance of surface tension has been well-appreciated in regards large lengthscale hydrophobic hydration, the Egelstaff and Widom length draws out the perhaps underappreciated role of compressibility to predict the critical separation at which different liquids will dewet. At the same time, if B60's isothermal compressibility was only half of its value- which would still be large- the EW length would be no different than that for H30. More liquids need to be investigated to see whether EW lengths offer a better predictive measure of dewetting distances beyond the surface tension trends shown in Figure 2.

## **5. CONCLUSION**

In this paper we use three members of these same classes of models to show hydration behavior for water confined between a pair of mesoscopic hydrophobic particles. While no model exhibits drying for any attraction strength between GB particles and the solvent, we do find that the various modified and SPC/E liquid models dewet the hydrophobic surface at different separation distances near purely repulsive GB particles. The hybrid H30 potential, which has the highest surface tension relative to all models examined here, sustains a sharper interface with a Gaussian distribution of bulk-like liquid densities, consistent with its smaller value of the EW length, and cavitates at shorter separations of the repulsive GB particles. By contrast the bent B60 potential is the least stable liquid between the repulsive GB particles, with a broad interface consistent with its low surface tension and non-Gaussian distribution biased toward low density cavities, consistent with its larger EW length, and evaporates at larger separations. The isotropic model does not show a non-contact

separation in which solvent is absent, likely due to its repulsive self-interactions that push the solvent onto the inert solutes.

**ACKNOWLEDGEMENTS.** RMLB thanks EPSRC (grants DR/S41562/01, GR/S181066/01 and EP/D029538/1) THG gratefully acknowledges a Schlumberger Fellowship while on sabbatical at Cambridge University, and research support under the DOE CPIMS program.

## 6. REFERENCES

- [1] P. R. ten Wolde, *J. Phys. Cond. Matter* 14, 9445 (2002).
- [2] D. Chandler, *Nature* 437, 640 (2005).
- [3] L. Pratt, D. Chandler, *J. Chem. Phys.* 67, 3683 (1977).
- [4] G. Hummer, S. Garde, A. E. García, A. Pohorille, L. R. Pratt. *Proc Natl Acad Sci USA* 93, 8951(1996).
- [5] H. S. Ashbaugh, L. R. Pratt. *Rev. Mod. Phys.* 78, 159 (2006)
- [6] P. Liu, X. Huang, R. Zhou, B. J. Berne, *Nature* 437, 159 (2005).
- [7] R. Zhou, X. Huang, C. Margulius, B. J. Berne, *Science* 305, 1605 (2004).
- [8] A. Pohorille, L.R. Pratt, *J. Am. Chem. Soc.* 112, 5066 (1990).
- [9] L. R. Pratt, A. Pohorille, *Proc Natl Acad Sci USA.* 89, 2995 (1992).
- [10] G. Hummer, S. Garde, *Phys. Rev. Lett.* 80, 4193 (1998).
- [11] J.D. Weeks, *Annu. Rev. Phys. Chem.* 53, 533 (2002)
- [12] X. Huang, C. J. Margulis, B. J. & Berne, *Proc. Natl Acad. Sci. USA* 100, 11953 (2003)
- [13] K. Lum, D. Chandler, J. D. Weeks, *J. Phys. Chem. B* 103, 4570 (1999).
- [14] K. Leung, A. Luzar, D. Bratko, *Phys. Rev. Lett.* 90, 65502 (2003).

- [15] A. Luzar, *J. Phys. Chem. B.* 108, 19859 (2004).
- [16] J. G. Gay, B. J. Berne, *J. Chem. Phys.* 74, 3316 (1981).
- [17] R. M. Lynden-Bell, P. G. Debenedetti. *J. Phys. Chem B* 109, 6527 (2005).
- [18] D. L. Bergman, R. M. Lynden-Bell, *Mol. Phys.* 99, 1011 (2001).
- [19] T. Head-Gordon, F. H. Stillinger. *J. Chem. Phys.* 98, 3313 (1993).
- [20] F. H. Stillinger, T. Head-Gordon. *Phys. Rev. E* 47, 2484 (1993).
- [21] T. Head-Gordon. *J. Am. Chem. Soc.* 117, 501 (1995).
- [22] H. J. C. Berendsen, J. R. Grigera, T. P. Straatsma. *J. Phys. Chem.* 91, 6269 (1987).
- [23] T. Head-Gordon, S.W. Rick, *Phys. Chem. Chem. Phys.* 9, 83 (2007).
- [24] A. K. Soper *Mol. Phys.* 99, 1503 (2001).
- [25] W. Smith, T. R. Forester, The Dlpoly 2.0 Manual, CCLRC, Daresbury Lab. Warrington (1995)  
see also: [http://www.dl.ac.uk/TCSC/Software/DL\\_POLY/main.html](http://www.dl.ac.uk/TCSC/Software/DL_POLY/main.html)
- [26] S. Nose, *J. Chem. Phys.* 81, 511 (1984).
- [27] W. G. Hoover, *Phys. Rev. A* 31, 1695, (1985)
- [28] G. J. Martyna, M. E. Tuckerman, M. L. Klein, *J. Chem. Phys.* 97, 2635 (1992).
- [29] H. C. Anderson, *J. Comp. Phys.* 52, 24 (1983).
- [30] J. P. Ryckaert, G. Ciccotti, H. J. C. Berendsen, *J. Comput. Phys.* 23, 327 (1977).
- [31] V. Kraeutler, W. F. van Gunsteren, P. H. Huenenberger, *J. Comput. Chem.* 22, 501 (2001).
- [32] H. W. Horn, W. C. Swope, J. W. Pitera, J. D. Madura, T. J. Dick, G. Hura, T. Head-Gordon. *J. Chem. Phys.* 120, 9665 (2004).
- [33] G. Hummer, N. Gronbech-Jensen, M. Neumann. *J. Chem. Phys.* 109, 2791 (1998).
- [34] J. Alexandre and R. M. Lynden-Bell, *Mol. Phys.* (2007) in press.
- [35] R. M. Lynden-Bell and T. Head-Gordon, *Mol. Phys.* 104, 3593 (2007).
- [36] P. Egelstaff, B. Widom, *J. Chem. Phys.* 53, 2667 (1970).



[37] T. Head-Gordon and S. Rick, *Phys. Chem. Chem. Phys.* 8, 83 (2007)

## FIGURE CAPTIONS

**Figure 1.** *Schematic of the Simulation Setup for the Gay-Berne particles whose centers are separated by distance,  $D$ . The size and shape of the ellipsoidal particles are controlled by parameters  $\sigma_{\parallel}$  and  $\sigma_{\perp}$ . See methods for further detail.*

**Figure 2.** *Critical Separation Distance  $D_c$  vs. Surface Tension.* Liquids with smaller values of the surface tension correlate with larger values of the critical separation at which drying occurs.

**Figure 3.** *Cylindrically averaged water densities for three of the solvent models between a pair of Gay-Berne particles separated at different distances.* (a) the H30 model sustains a much sharper interface with the Gay-Berne particles as compared to (b) SPC/E and (c) the B60 model which has the broadest interface at the Gay-Berne particle surfaces.

**Figure 4.** *Cavity statistics collected at the center between the Gay-Berne particles for the H30 Model.* (a) when separated at a distance  $D \sim D_c$ , and (b) when separated at a distance  $D > D_c$ .

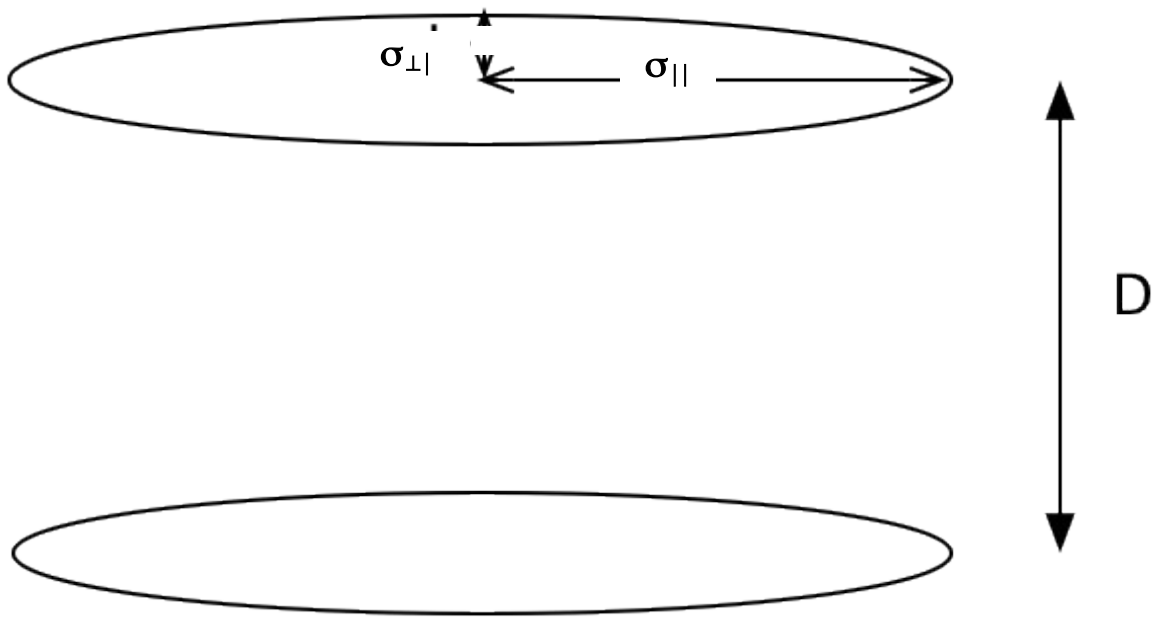
**Figure 5.** *Cavity statistics collected at the center between the Gay-Berne particles for the B60 Model.* (a) when separated at a distance  $D \sim D_c$ , and (b) when separated at a distance  $D > D_c$ .

TABLE 1. Potential parameters for modified water models

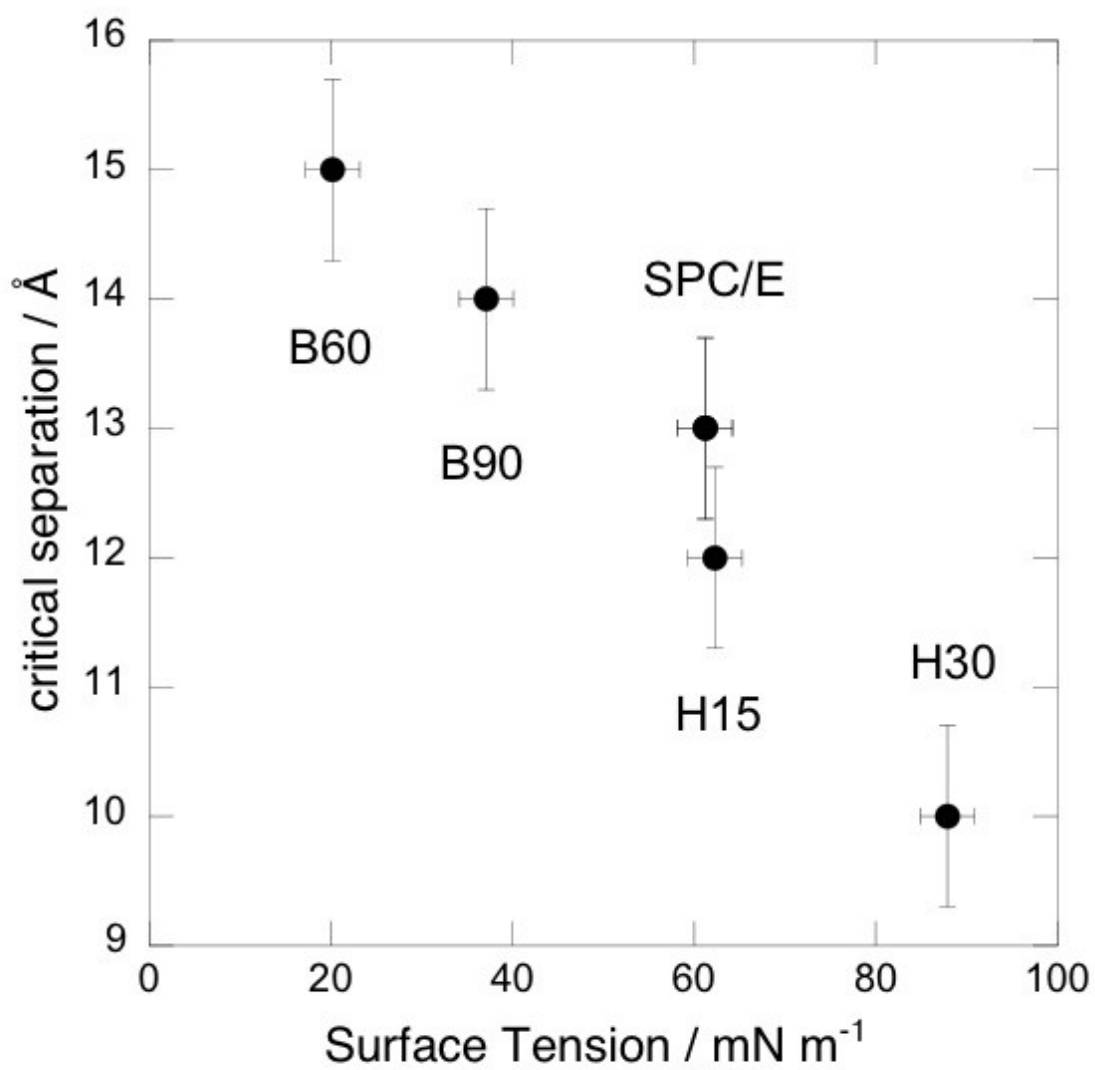
Property	SPC/E	H15	H30	B90	B60
$q_o/e$	-0.8476	-0.8476	-0.8476	-0.8476	-0.8476
$\epsilon_{oo}/\text{kJ mol}^{-1}$	0.6502	0.9753	1.9505	0.6502	0.6502
$\sigma_{oo}/\text{\AA}$	3.165	3.165	3.165	3.05	2.92
$\angle \text{HOH}$	109.5	109.5	109.5	90.0	60.0
$r_{OH}/\text{\AA}$	1.0	1.0	1.0	0.817	0.667
Dipole/ D	2.35	2.35	2.35	2.35	2.35

TABLE 2. Liquid and solvation properties of modified water models at 298K.

Property	SPC/E	H15	H30	B90	B60	Iso
$D_c (\text{\AA})$	13	12	10	14	15	8
Potential Energy / $\text{kJ/mol}^{-1}$	-46.3	-42.3	-41.7	-33.7	-35.9	3.2
Surface Tension / $\text{dyn cm}^{-1(34)}$	61.2	62.3	87.9	37.1	20.2	0.2
$\kappa_T / 10^{-6} \text{ atm}^{-1(22, 37)}$	51.7		25.0		230.7	
Egelstaff-Widom Length / $\text{\AA}$	0.316		0.219		0.466	
$T_c/\text{K}^{(a)}$	640	631	678	508	520	
Gmax(r)	1.5		2.6		1.0	2.6



**Figure 1. Head-Gordon and Lynden-Bell**



**Figure 2. Head-Gordon and Lynden-Bell**

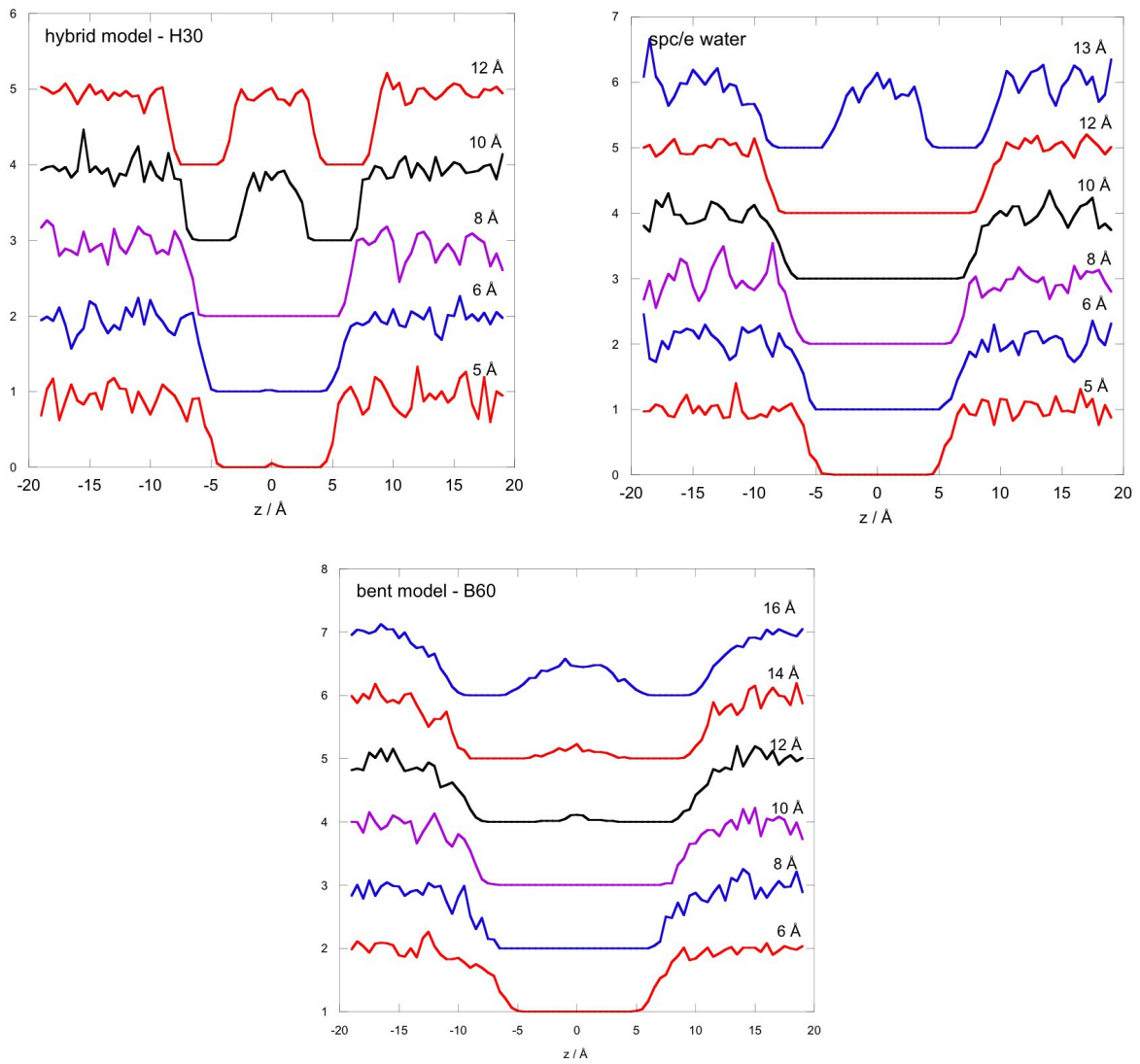
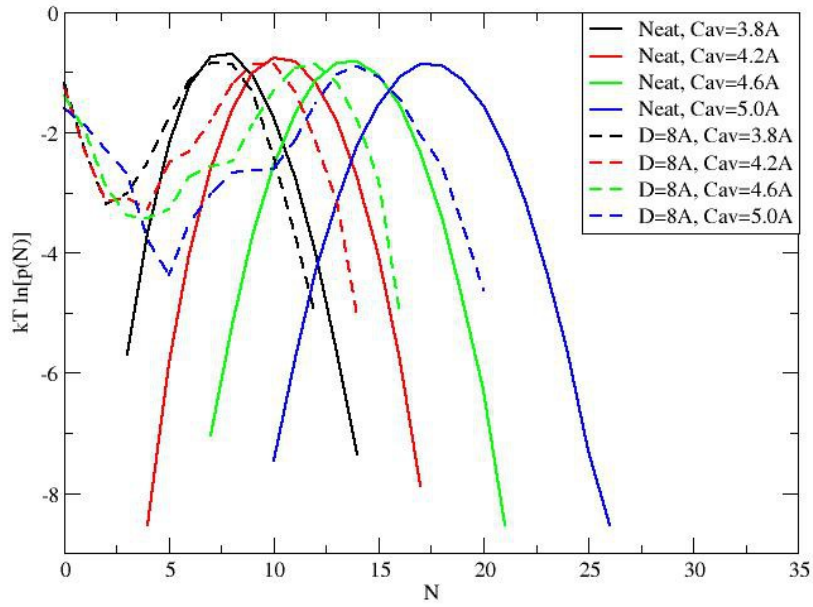


**Figure 3. Lynden-Bell and Head-Gordon**

H30 GB and Neat



H30 GB and Neat

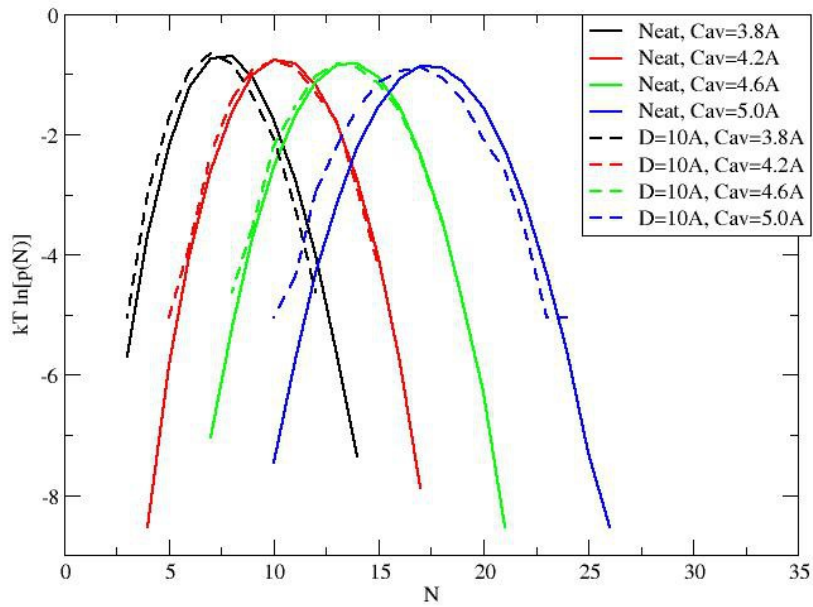
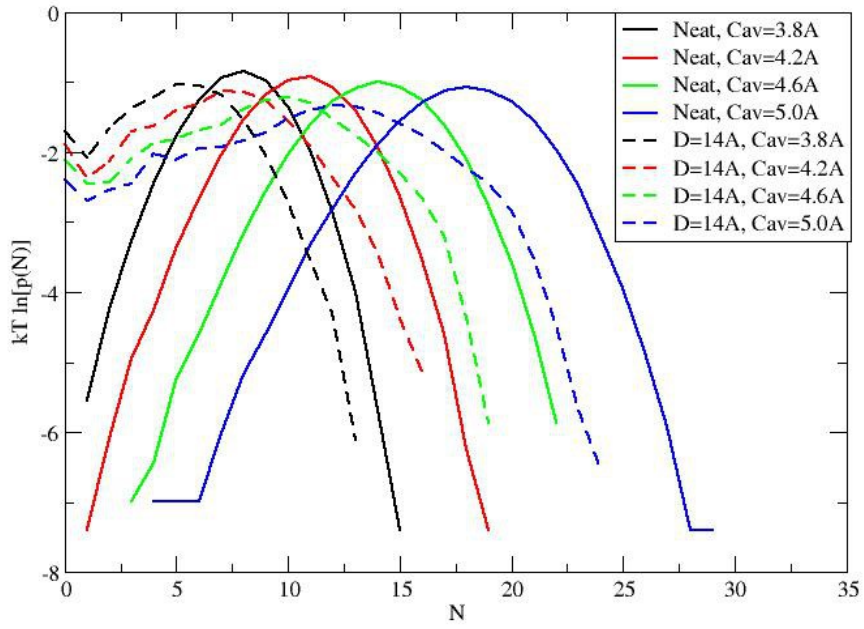


Figure 4. Lynden-Bell and Head-Gordon

B60 GB and Neat



B60 GB and Neat

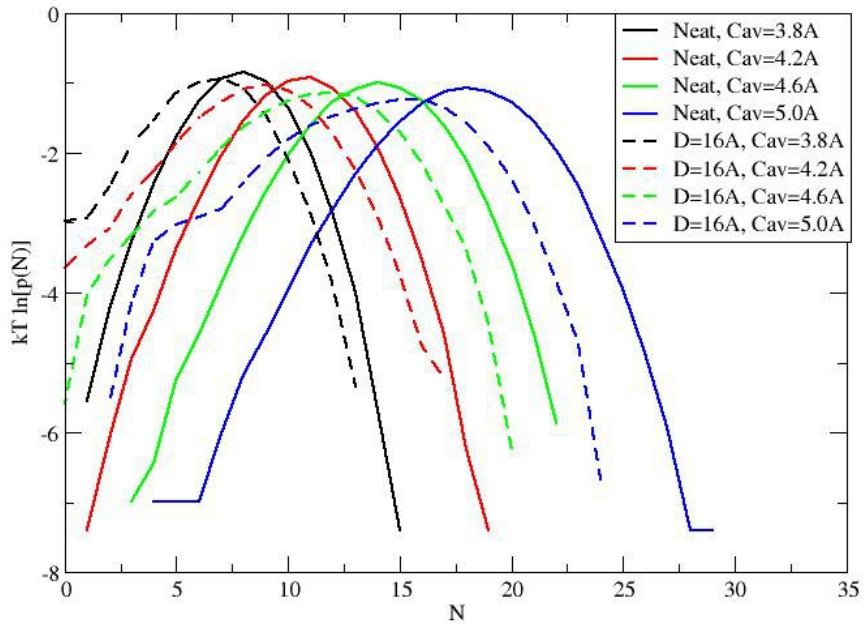


Figure 5. Lynden-Bell and Head-Gordon